

# Training Self-Supervised Depth Completion Using Sparse Measurements and a Single Image

Rizhao Fan

Zhigen Li

Heping Li

Ning An

## Abstract

*Depth completion is an important vision task, and many efforts have been made to enhance the quality of depth maps from sparse depth measurements. Despite significant advances, training these models to recover dense depth from sparse measurements remains a challenging problem. Supervised learning methods rely on dense depth labels to predict unobserved regions, while self-supervised approaches require image sequences to enforce geometric constraints and photometric consistency between frames. However, acquiring dense annotations is costly, and multi-frame dependencies limit the applicability of self-supervised methods in static or single-frame scenarios. To address these challenges, we propose a novel self-supervised depth completion paradigm that requires only sparse depth measurements and their corresponding image for training. Unlike existing methods, our approach eliminates the need for dense depth labels or additional images captured from neighboring viewpoints. By leveraging the characteristics of depth distribution, we design novel loss functions that effectively propagate depth information from observed points to unobserved regions. Additionally, we incorporate segmentation maps generated by vision foundation models to further enhance depth estimation. Extensive experiments demonstrate the effectiveness of our proposed method.*

## 1. Introduction

Depth completion aims to estimate dense depth maps from sparse depth measurements, addressing the inherent limitations of depth sensing technologies. Active depth sensing techniques, such as LiDAR and time-of-flight sensors, directly measure scene depth but produce sparse and incomplete depth maps [14, 39]. Passive methods, including stereo depth estimation and structure-from-motion (SfM), infer depth from natural image cues but struggle in textureless or dynamic environments, leading to unreliable and sparse depth estimates [36]. These limitations make depth completion a critical task for applications such as scene reconstruction and robotic perception.

To densify sparse depth data, early depth completion methods relied on explicit geometric assumptions, hand-crafted features, or optimization-based techniques, such as bilinear interpolation and joint bilateral filtering [22, 32, 38]. With the advancement of deep learning, learning-based depth completion approaches have achieved significant improvements [5, 9, 16, 19, 23, 31, 53, 55]. Supervised depth completion methods [9, 23, 33, 55] leverage densely annotated depth maps as supervision signals to optimize neural networks. Many of these methods utilize RGB images as additional guidance to propagate depth information from observed points to unobserved regions. However, obtaining densely labeled depth data is expensive and time-consuming [2, 14], limiting the scalability of supervised approaches.

To mitigate this limitation, self-supervised depth completion methods have been explored [1, 8, 11–13, 30, 43, 44, 49, 52]. These methods eliminate the need for dense depth annotations by enforcing photometric consistency between image pairs, using sparse depth measurements as weak supervision. However, existing self-supervised methods typically require multiple images to establish geometric constraints, making them less applicable in scenarios where only a single image is available or in static environments. Despite extensive research in depth completion, no prior work has addressed the challenge of completing depth using only sparse depth measurements and their corresponding single image during training. This forms the core contribution of our research.

In this paper, we propose a novel self-supervised depth completion paradigm (SelfDC) that eliminates the reliance on dense depth labels and geometric or photometric consistency constraints between adjacent frames during training. Our method requires only sparse depth measurements and synchronized RGB image, making it more flexible and cost-effective. In inference time, the method only requires sparse depth measurements and synchronized RGB images. Our approach incorporates segmentation masks derived from vision foundation model for image segmentation [18, 21] to assist self-supervised depth completion. By leveraging these masks, our method focuses on depth estimation across

object surfaces, improving structural consistency in the predicted depth. Building on the principle of depth smoothness, we introduce a Local Gradient Constraint Loss, which penalizes excessively large local depth gradients while promoting overall depth consistency. This facilitates more effective propagation of observed depth measurements into unobserved regions. Additionally, we propose a Selective Mask-Aware Smoothness Loss to further refine depth smoothness within object regions, ensuring more effective gradient propagation. Extensive experiments on the NYU Depth v2 and KITTI Depth Completion datasets demonstrate the effectiveness of our approach, showcasing its significant potential in depth completion.

Our main contributions can be summarized as follows:

- We propose, to the best of our knowledge, the first self-supervised depth completion framework that relies solely on sparse depth measurements and synchronous RGB images during training, eliminating the need for ground truth depth or image sequences.
- We introduce a novel **Local Gradient Constraint Loss**, which effectively propagates depth values from observed regions to unobserved areas, significantly improving prediction accuracy.
- We design a **Selective Mask-Aware Smoothness Loss** that prioritizes regions with significant gradient variations, leading to more natural and consistent depth predictions.
- Extensive experiments demonstrate the effectiveness of our approach, achieving state-of-the-art performance and validating the feasibility of our method.

## 2. Related Work

In this section, we review self-supervised depth estimation approaches relevant to our proposal, categorized into (1) supervised depth completion, and (2) self-supervised depth completion.

### 2.1. Supervised Monocular Depth Completion

In recent years, depth completion based on sparse depth measurements by LiDAR or SfM has gained increasing attention, particularly methods guided by color images, leading to a significant increase in related approaches. Ma *et al.* [29, 30, 33] concatenate the depth map and RGB image as input in early fusion manner to a deep network for processing. Other methods [16, 23, 25, 37] utilize late fusion strategies to merges image features and depth features to realize depth completion. Some studies [31, 35, 46] propose multi-task approaches by combining depth maps with estimated surface normals or semantics. For example, Qiu *et al.* [35] use surface normals as intermediate representations to fuse with sparse depth data. Other studies [3, 4, 50] explore geometric information from 3D point clouds. Transformer

architectures [54, 56] have also been introduced to facilitate multi-modal fusion through attention mechanisms [28, 40].

Depth completion based on spatial propagation networks (SPNs) [5–7, 24, 33, 47] have become a hot research topic, iteratively refining predicted depth by aggregating reference and neighboring pixels. The initial SPN [26] updates each pixel using three neighboring pixels from the previous row or column. CSPN [5] improves upon this by simultaneously updating all pixels with fixed local neighbors. To incorporate non-local neighbors, DySPN [24] and NL-SPN [33] learn offsets relative to the regular grid. GraphCSPN [27] integrates 3D information into the update process, while LRRU [41] employs multi-scale guidance features to adaptively guide the prediction of neighbors and weights throughout the update process.

### 2.2. Self-Supervised Monocular Depth Completion

A new trend [1, 8, 11–13, 30, 44, 49, 51] focuses on estimating dense depth prediction from image sequences and LiDAR data (e.g., single-beam and 4-beam LiDAR) in a self-supervised manner, thereby minimizing deployment costs. This problem can be viewed as self-supervised depth completion, which relies on the geometric relationships between adjacent images and depth consistency between inputs and outputs, rather than on dense depth labels adopted in supervised depth completion methods. This approach can also be seen as LiDAR-assisted self-supervised depth estimation. SelfDeco [8] develop a robust self-supervised depth completion framework for challenging indoor environments. Ma *et al.* [30] proposed a self-supervised training framework that uses pose estimation based on the PnP method to process sequences of color and sparse depth images. Feng *et al.* [13] presented a representative solution in this field, using a two-stage network to infer dense depth maps. Fan *et al.* [11] used a lightweight yet effective self-supervised network to process few-beam LiDAR data and a single image. DesNet [49] disintegrates the absolute depth into relative depth prediction and global scale estimation which propagates dense depth reference into the sparse target to help unsupervised depth completion. Fan *et al.* [12] proposed a self-supervised depth completion method that relies on the photometric consistency between few-beam LiDAR data and multiple image frames.

Nonetheless, our proposed method differs from the aforementioned approaches because it does not rely on dense depth labels or require geometric relationships between adjacent images for model optimization. Instead, it leverages only sparse depth information and image data to achieve depth completion in the training. This distinctive design not only addresses the inherent limitations of both supervised and self-supervised methods but also enhances the practicality and efficiency of the depth estimation process.

### 3. Methodology

We now present our proposal: Sec. 3.1 introduces our self-supervised depth completion framework. Then, we introduce the proposed loss functions, with Sec. 3.2 detailing the Local Gradient Constraint Loss and Sec. 3.3 presenting the Selective Mask-Aware Smoothness Loss. Finally, Sec. 3.4 provides an overview of the overall loss functions.

#### 3.1. Framework

Let  $I \in \mathbb{R}^{H \times W \times 3}$  represent a color image and  $S \in \mathbb{R}^{H \times W}$  denote the corresponding sparse depth map. Our goal is to generate dense depth maps  $\hat{D} \in \mathbb{R}^{H \times W}$  by leveraging the complementary information embedded in  $I$  and  $S$ . While the color image  $I$  provides rich contextual information, sharp object boundaries, and high-level semantics, its excessive texture details can hinder the effective propagation of depth information across the image. To address this issue, we introduce a segmentation mask,  $M \in \mathbb{R}^{H \times W}$ , which helps partition the scene into semantically consistent regions.

In the training, our framework adopts a multi-task learning strategy, jointly predicting depth and segmentation maps during training, as shown in Fig. 1. For the Depth Decoder branch, We follow the approach described in [29, 33] to predict the depth map and further refine it using the Non-local Spatial Propagation Network (NLSPN) [33]. The Segmentation Decoder branch shares the same architectural structure as the depth decoder but uses a different prediction head to generate segmentation outputs. The segmentation map  $M$  generated by the segmentation foundation model [18, 21] serves as pseudo-labels to supervise the segmentation prediction  $\hat{M}$  in the training process. In our task,  $M$  offers semantically consistent regions, capturing object boundaries and structural details in the scene. By leveraging  $M$  as auxiliary guidance, we enhance the accuracy and structural consistency of depth estimation. During inference, the segmentation prediction branch is removed.

#### 3.2. Local Gradient Constraint Loss

In both supervised and self-supervised depth completion networks, as training progresses and the model is optimized, depth information gradually propagates from observed points to unobserved regions. This propagation is driven by depth supervision and geometric constraints, resulting in increasingly smooth depth variations across object surfaces [9–12, 29]. However, in the novel self-supervised depth completion task we propose, propagating depth information from observed points to surrounding unobserved areas remains a significant challenge due to the absence of explicit depth supervision and geometric constraints between adjacent images.

As training progresses and prediction accuracy improves, depth information propagates more smoothly from

observed points to the surrounding areas, resulting in increasingly refined depth prediction. Consequently, the depth gradient becomes progressively smoother. Based on this observation, we propose a novel loss function to regularize the depth gradient. Specifically, this loss penalizes locations with excessively large gradients, encouraging smoother depth propagation from sparse observation points to surrounding areas. Since object edges naturally exhibit large depth gradients, we introduce the segmentation mask  $M$ , for more precise edge guidance. Unlike edge-aware smoothness losses that rely on image-derived edges, segmentation masks provide clearer object boundaries and semantic information, which are often more distinct and reliable than edges detected from RGB images. At object boundaries—where transitions between different semantic regions occur—depth values may change sharply. Preserving these edge gradients is crucial to prevent excessive smoothing.

However, from a global perspective of the depth map, as shown in Figure 2, certain regions, such as the walls of a long hallway directly facing the camera, tend to exhibit significant depth gradients, aside from object boundaries. If we penalize only the largest gradients across the entire depth map, it may lead to insufficient constraints in some flat areas. To address this issue, inspired by Swin Transformer [28] and WCL [10], we propose a **Local Gradient Constraint Loss**. Unlike penalizing the largest gradients globally, we divide the depth map into non-overlapping windows of size  $W \times W$ . Within each window, we select the top  $N$  points with the largest depth gradients (corresponding to the top 2% of all points in the  $W \times W$  window) and apply penalties to these gradients. This approach allows for effective control of depth propagation within localized regions, preventing over-smoothing while preserving the structural integrity of the scene.

The loss function can be expressed as:

$$L_{gc} = \frac{1}{K} \cdot \frac{1}{N} \sum_{k=1}^K \sum_{(i,j) \in \mathcal{S}_k} |\nabla D(i,j)| \quad (1)$$

where:  $K$  is the total number of local windows into which the depth map is divided,  $\mathcal{S}_k$  represents the set of top  $N$  gradient points within the  $k$ -th local window,  $|\nabla D(i,j)|$  denotes the absolute gradient of the depth map at pixel  $(i,j)$ .

#### 3.3. Selective Mask-Aware Smoothness Loss

In this work, we propose a novel depth smoothness loss, termed **Selective Mask-Aware Smoothness Loss** ( $L_{sms}$ ), which extends **Edge-Aware Smoothness Loss** ( $L_{smooth}$ ), defined as:

$$L_{smooth} = \sum_{i,j} |\nabla D(i,j)| \cdot e^{-|\nabla I(i,j)|} \quad (2)$$

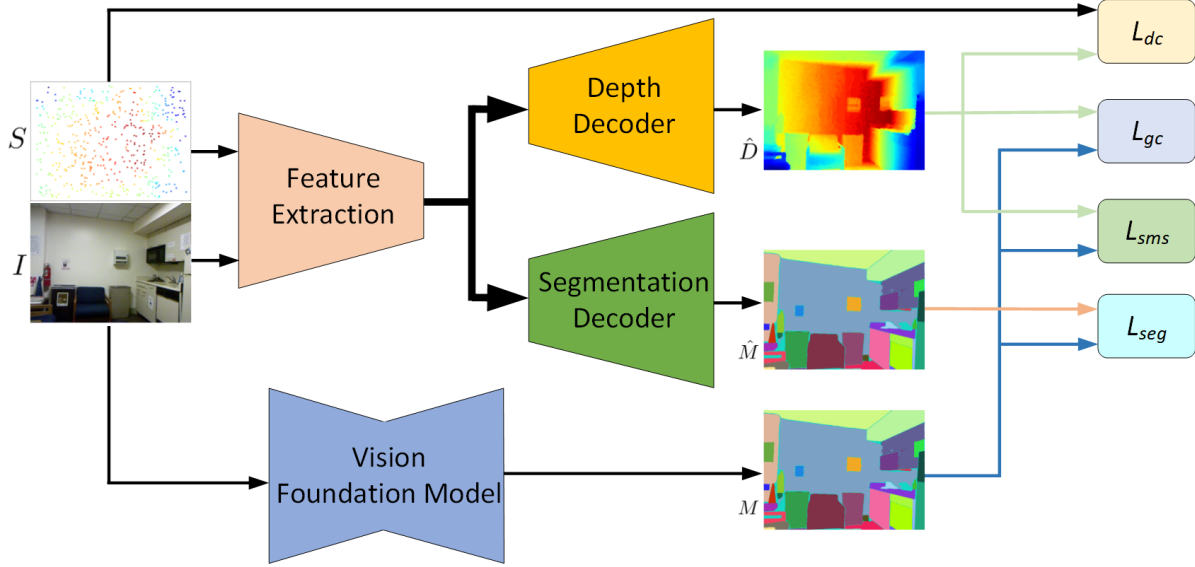


Figure 1. **Our proposed framework.** Our network composed of feature extraction, depth decoder and segmentation decoder. In the training, we use **Segment Anything** to obtain segmentation mask as pseudo label for the segmentation prediction. In the inference, only the feature extraction and depth decoder are kept.

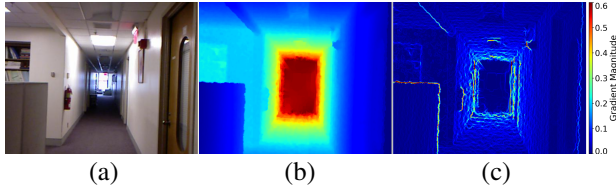


Figure 2. **Examples of depth gradient.** from left to right: RGB, depth GT, depth gradient map. It can be observed that the depth gradient exhibits high values even in the corridor.

Unlike  $L_{smooth}$ , which enforces smoothness constraints globally across the entire image,  $L_{sms}$  introduces a segmentation-guided strategy that applies smoothness within individual regions defined by segmentation masks. This approach preserves structural boundaries and maintains object integrity by smoothing depth gradients only within object-specific regions.

Specifically,  $L_{sms}$  replaces the image gradient weighting term in  $L_{smooth}$  with segmentation masks to prioritize smoothness within each region. Instead of averaging all depth gradients, it selects the top 40% of gradients within each segmented region, focusing on significant variations. The loss is then calculated as the mean of these prioritized gradients, effectively penalizing large depth anomalies while maintaining intra-region consistency. By confining smoothness computation to segmentation regions,  $L_{sms}$  avoids over-smoothing across object boundaries and enhances depth propagation within complex geometries and occluded areas, resulting in more accurate depth completion.

The loss function is formulated as follows:

$$L_{sms} = \frac{1}{|\mathcal{S}|} \sum_{s \in \mathcal{S}} \frac{1}{|\mathcal{Q}_s|} \sum_{p \in \mathcal{Q}_s} (|\partial_x D(p)| + |\partial_y D(p)|), \quad (3)$$

where,  $\mathcal{S}$  is the set of segmentation regions,  $\mathcal{Q}_s$  is the top 40% pixels with the highest depth gradients in region  $s$ , defined as:

$$\mathcal{Q}_s = \text{Top-40\%} (\{|\partial_x D(p)| + |\partial_y D(p)| \mid p \in \mathcal{P}_s\}), \quad (4)$$

where,  $\mathcal{P}_s$  is the set of all pixels in region  $s$ ,  $\partial_x D(p)$  and  $\partial_y D(p)$  is depth gradients along the  $x$  and  $y$  directions.

### 3.4. Loss Functions

For optimizing the model, in addition to the loss functions described above, we employ the following two loss functions.”

**Depth Consistency Loss.** This loss  $L_{dc}$  is commonly used in self-supervised depth completion methods [1, 8, 11, 13, 30]. It ensures that the predicted dense depth map aligns with the input sparse depth measurements. Specifically, the loss is calculated on valid (non-zero) depth points:

$$L_{dc} = \frac{1}{|V|} \sum_{i \in V} \|\hat{D}(i) - S(i)\|_1 \quad (5)$$

where  $V$  represents the set of valid depth points.

**Segmentation Loss.** We use the cross-entropy loss to measure the discrepancy between the predicted segmentation map and the ground truth pseudo-labels:

$$L_{seg} = -\frac{1}{N} \sum_{i=1}^N \sum_{c=1}^C y_i^c \log(p_i^c) \quad (6)$$

where  $N$  is the total number of pixels,  $C$  is the number of classes,  $y_i^c$  is the ground truth probability of pixel  $i$  belonging to class  $c$ , and  $p_i^c$  is the predicted probability for the same.

The overall loss function is defined as:

$$L_{total} = L_{dc} + \alpha L_{seg} + L_{gc} + L_{sms} \quad (7)$$

where  $\alpha$  is a weighting factor for the segmentation loss. Empirically, we set  $\alpha = 0.1$ .

## 4. Experiments

We conducted extensive experiments to evaluate our proposed SelfDC on standard depth completion benchmarks and compare it with state-of-the-art (SOTA) solutions, then carry out ablation studies to analyze different parts of our proposed approach.

### 4.1. Experimental Setup

**Datasets.** We conduct standard depth completion evaluations on three widely-used benchmarks: NYU Depth v2 (NYUD-v2) [36] and KITTI Depth Completion (KITTI-DC) [14, 39]. These datasets encompass diverse indoor and outdoor scenes, following established sampling protocols for generating input sparse depth maps [29, 33].

NYU Depth v2 contains RGB-D data captured by a Kinect sensor across 464 indoor scenes. Utilizing the official dataset split, we employ 249 scenes for training and 215 for testing. Consistent with standard practices [24, 29, 33], we sample approximately 50,000 images from the training set, resizing the original  $480 \times 640$  images to half resolution followed by center cropping to  $228 \times 304$ . Evaluation is performed on the official test set comprising 654 images.

The **KITTI dataset** [14], a prominent benchmark in autonomous driving research, provides extensive outdoor scene data. Its depth completion subset (**KITTI-DC**) [39] offers sparse depth maps from a Velodyne LiDAR HDL-64e, color images, and corresponding semi-dense ground truth depth maps. The sparse depth maps contain approximately 5.9% valid depth measurements, while the ground truth provides 16% coverage. The dataset is partitioned into 85,895 training frames, with an additional 1,000 frames each for validation and testing (the latter having withheld ground truth).

**Implementation Details.** Our proposed method is implemented using PyTorch [34] and trained on a machine equipped with 8 NVIDIA RTX 4090D GPUs. For all experiments, we use the ADAM optimizer [20] with  $\beta_1 = 0.9$ ,  $\beta_2 = 0.999$ , and an initial learning rate of 0.001. We

employ ResNet34 [15] as the backbone for our encoder-decoder network. Due to the sensitivity of our method to noise in the input sparse depth measurements, we preprocess the KITTI-DC datasets by filtering out a portion of the noise to mitigate its impact, following [11]. For the NYU Depth v2 dataset, we use Segment Anything[21], and for the KITTI dataset, we employ OneFormer[18].

**Evaluation Metrics.** We evaluate depth completion performance using standard metrics as defined in [29, 33]. These metrics include Root Mean Squared Error (RMSE), Absolute Relative Error (Abs Rel), and accuracy under thresholds ( $\delta < 1.25$ ,  $\delta < 1.25^2$ , and  $\delta < 1.25^3$ ). For the KITTI Depth Completion (KITTI-DC) test set, we adopt the official evaluation metrics: RMSE, Mean Absolute Error (MAE), inverse RMSE (iRMSE), and inverse MAE (iMAE). Detailed mathematical formulations of these metrics are provided in the supplementary material. Depth values are evaluated within predefined maximum ranges: 80 meters for KITTI datasets and 10 meters for NYUD-v2.

### 4.2. Results on NYUD-v2 and KITTI

**NYUD-Depth-v2 Dataset.** Table 1 presents the quantitative results on the NYU Depth v2 dataset, comparing our proposed SelfDC method against both early supervised learning approaches and state-of-the-art self-supervised depth completion methods. Our evaluation focuses on performance with varying numbers of sparse depth samples (200, 500, 1000 and 2000). When compared to supervised depth completion methods utilizing the same number of sparse depth samples, SelfDC demonstrates competitive performance, achieving accuracy levels comparable to several early supervised techniques. Notably, in comparison with existing self-supervised approaches, SelfDC consistently outperforms all competitors, showcasing superior effectiveness and robustness across different levels of sparse depth inputs. These results highlight SelfDC’s ability to achieve high accuracy without relying on dense ground truth depth data, establishing a new paradigm for self-supervised depth completion.

Figure 3 provides a qualitative comparison of our method with several existing works. Sparse depth pixels were randomly sampled from dense depth images and used as input alongside corresponding RGB images. When compared to early supervised learning method (S2D), SelfDC produces clearer and more accurate depth predictions, particularly in capturing fine structural details such as the shape edges of sofa and cabinet. This improvement underscores the benefits of our mask-guided methods. In comparison with state-of-the-art methods (NLSPN), SelfDC achieves competitive results, though some limitations are observed. For instance, our method occasionally struggles with fine-grained details, such as intricate patterns on bookshelves. However, these limitations become less pronounced as the

Method	Depth Samples	Training	RMSE ↓	REL ↓	$\delta < 1.25 \uparrow$	$\delta < 1.25^2 \uparrow$	$\delta < 1.25^3 \uparrow$
Liao et al.[29](ICRA 2017)	225	S	0.442	0.104	87.8	96.4	98.9
S2D[29](ICRA 2018)	200	S	0.230	0.044	97.1	99.4	99.8
S2D[29](ICRA 2018)	500	S	0.204	0.043	97.8	99.6	99.9
DepthCoeff[17] (CVPR 2019)	500	S	0.118	0.013	99.4	99.9	-
CSPN [5] (ECCV 2018)	500	S	0.117	0.016	99.2	99.9	100.0
CSPN++ [7] (AAAI 2020)	500	S	0.116	-	-	-	-
DeepLiDAR [35] (CVPR 2019)	500	S	0.115	0.022	99.3	99.9	100.0
DepthNormal [46] (ICCV 2019)	500	S	0.112	0.018	99.5	99.9	100.0
NLSPN [33] (ECCV 2020)	500	S	0.092	0.012	99.6	99.9	100.0
ACMNet [55] (TIP 2021)	500	S	0.105	0.015	99.4	99.9	100.0
RigNet [48] (ECCV 2022)	500	S	0.090	0.013	99.6	99.9	100.0
DFU [42] (ICCV 2023)	500	S	0.091	0.011	99.6	99.9	100.0
Yang et al. [51] (CVPR 2019)	200	SS	0.569	0.171	-	-	-
Yoon et al. [52] (IROS 2020)	200	SS	0.309	-	-	-	-
Ma et al. [30] (ICRA 2019)	200	SS	0.230	0.044	97.1	99.4	99.8
Ma et al. [30] (ICRA 2019)	500	SS	0.271	0.068	-	-	-
Selfdeco [8] (ICRA 2021)	200	SS	0.240	0.048	96.6	99.4	99.9
Selfdeco [8] (ICRA 2021)	500	SS	0.178	0.033	98.1	99.7	100.0
KBNet* [43] (ICCV 2021)	~ 1500	SS	0.197	-	-	-	-
DesNet* [49] (AAAI 2023)	~ 1500	SS	0.188	-	-	-	-
SelfDC	200	SS-M	0.229	0.044	96.9	99.4	100.0
SelfDC	500	SS-M	0.141	0.023	98.9	99.8	100.0
SelfDC	1000	SS-M	0.107	0.015	99.4	99.9	100.0
SelfDC	2000	SS-M	0.085	0.012	99.6	100.0	100.0

Table 1. **Quantitative Results on NYU Depth-v2 test split.** Evaluation metrics include RMSE (in meters), REL, and accuracy under  $\delta$  thresholds. Methods are categorized into three groups: **Supervised Depth Completion Methods:** Listed in the top section of the table. **Self-Supervised Depth Completion Methods:** Listed in the middle section of the table. **Our Proposed SelfDC:** Listed in the bottom section of the table. Training types: S = Supervised, SS = Self-Supervised using image sequences, SS-M = Self-Supervised with Mask-Aware strategy. \*: Methods with inputs at  $640 \times 480$  resolution.

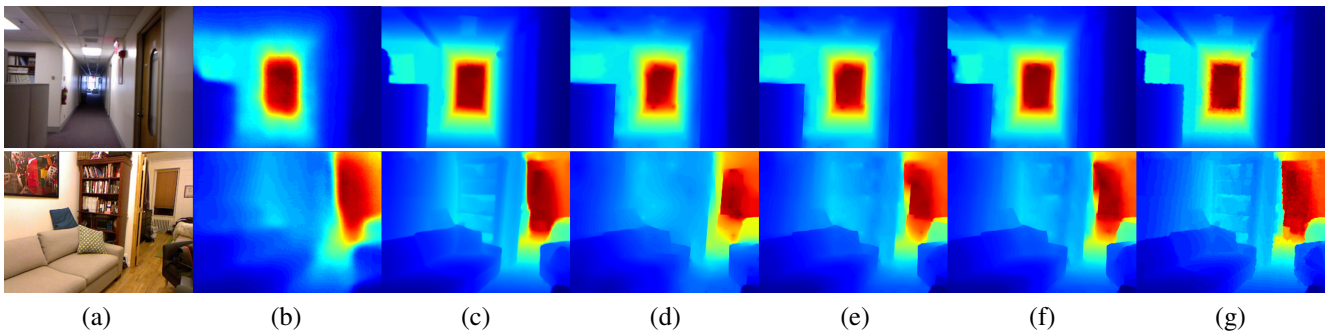


Figure 3. Qualitative results on NYUD-v2 test split. From left to right: (a) RGB images; (b) S2D [29] prediction with 200 samples; (c) NLSPN [33] prediction with 500 samples; (d) SelfDC prediction with 200 samples; (e) SelfDC prediction with 500 samples; (f) SelfDC prediction with 1000 samples; (g) ground truth depth.

number of sparse depth samples increases. Overall, our method demonstrates significant potential, offering a robust and effective solution for self-supervised depth completion.

**KITTI-DC Dataset.** The quantitative results on the KITTI Depth Completion Dataset are presented in Table 2, which summarizes the evaluation outcomes. Our proposed SelfDC method is compared with early supervised learning approaches utilizing RGB-D inputs. Notably, under the

same LiDAR beam configuration, SelfDC achieves performance on par with both early supervised depth completion methods and state-of-the-art (SOTA) self-supervised depth completion approaches. The results in this table further validate the effectiveness of our method in outdoor scenarios.

Method	RMSE	MAE	iRMSE	iMAE
Uhrig et al. [39] (3DV 2017)	1601.33	481.27	4.94	1.78
Ma et al.[30] (ICRA2019)	814.73	249.95	2.80	1.21
Ma et al. [30] (ICRA 2019)	1299.85	350.32	4.07	1.57
DDP [51] (CVPR2019)	1263.19	343.46	3.58	1.32
VOICED [44](RAL 2020)	1169.97	299.41	3.56	1.20
Yoon et al.[52] (IROS 2020)	1593.37	547.00	28.0	2.36
FusionNet [45](RAL 2021)	1182.81	286.35	3.55	1.18
KBNet [43] (ICCV 2021)	1068.07	258.36	3.01	1.03
DesNet [49] (AAAI 2023)	938.45	266.24	2.95	1.13
SelfDC	1206.97	353.93	3.74	1.48

Table 2. **Comparison with supervised depth estimation methods on the KITTI-DC test set.** The evaluation metrics include RMSE and MAE, both reported in millimeters (mm), and iRMSE, reported in 1/km. All the methods compared are depth completion approaches that utilize RGB images along with LiDAR data from the same beam configuration. Supervised Depth Completion Methods: Listed in the top section of the table. Self-Supervised Depth Completion Methods: Listed in the middle section of the table. Our Proposed Approach: Represented in the bottom section of the table

Method	$L_{seg}$	$L_{sms}$	$L_{gc}$	RMSE	REL
1				3.046	0.978
2	✓			2.909	0.978
3		✓		0.263	0.055
4			✓	0.166	0.027
5	✓	✓		0.251	0.051
6	✓		✓	0.164	0.028
7		✓	✓	0.158	0.027
8	✓	✓	✓	0.141	0.023

Table 3. **Performance comparison of the baseline and its variants with different modules.** Lower values indicate better performance. **Note:** Segmentation branch: Segmentation module,  $L_{seg}$ : Segmentation loss,  $L_{sms}$ : Selective Mask-Aware Smoothness Loss,  $L_{gc}$ : Local Gradient Constraint Loss.

### 4.3. Ablation Study

We perform a series of ablation studies to further show the effectiveness of our proposed method. The training and testing are all performed on the NYU depth v2 dataset.

**Effectiveness of Each Modules:** We investigate the effectiveness of various design aspects of our proposed SelfDC. Table 3 summarizes the ablation study results. **Method 1** serves as the baseline, containing only the depth branch and depth consistency loss. It performs poorly, providing minimal contribution to depth completion. Adding the segmentation branch with  $L_{seg}$  leads to moderate improvements over the baseline.  $L_{gc}$  shows the most significant enhancement, effectively propagating sparse depth

Methods	Constraint Basis	Window Size	RMSE	REL
1	M	Full	0.179	0.032
2	M	$128 \times 128$	0.250	0.051
3	M	$64 \times 64$	0.171	0.031
4	M	$16 \times 16$	0.148	0.025
5	M	$8 \times 8$	0.141	0.023
6	I	$8 \times 8$	0.149	0.025

Table 4. **Evaluation of different window sizes for  $L_{gc}$ .** The table reports RMSE and REL for each setting. The **Constraint Basis** column indicates the input used for gradient extraction: segmentation mask (M) or image (I). Methods represent different configurations of gradient constraints: Method 1 applies constraints over the entire depth map (Full), while Methods 2~5 use segmentation mask (M) as the constraint basis with window sizes of  $128 \times 128$ ,  $64 \times 64$ ,  $16 \times 16$ , and  $8 \times 8$  pixels, respectively. Method 6 uses the image (I) as the constraint basis with an  $8 \times 8$  window size.

measurements and substantially reducing RMSE and REL (Methods 4, 6, 7, and 8).  $L_{sms}$  also improves performance but to a lesser extent than  $L_{gc}$ . When combined with  $L_{gc}$ , it offers additional refinement (Methods 7 and 8). Overall, the best performance is achieved by combining all three components ( $L_{seg}$ ,  $L_{sms}$ , and  $L_{gc}$ ), demonstrating their complementary effects.

**Local Gradient Constraint Loss:** We utilize  $L_{gc}$  to propagate observed depth values to neighboring regions. To investigate the impact of window size, we evaluate different sizes as shown in Table 4, ranging from the entire size to  $128 \times 128$ ,  $64 \times 64$ ,  $16 \times 16$ , and  $8 \times 8$  pixels. The results show that applying  $L_{gc}$  over the entire depth map performs poorly (Method 1), while smaller windows improve accuracy, with  $8 \times 8$  yielding the best results (Method 5). This indicates that localized gradient constraints enhance depth propagation. We also compare two gradient basis: segmentation mask (M) and image (I). The segmentation mask consistently outperforms the image (Methods 5 vs. 6), likely due to reduced interference from texture details. These findings underscore the importance of choosing appropriate window sizes and smoothness bases for  $L_{gc}$ .

**Selective Mask-Aware Smoothness Loss:** We employ  $L_{sms}$  to enforce depth map smoothness. To evaluate its effectiveness, we compare it with several other methods. As shown in Table 5, mask-guided methods significantly outperform image-based smoothing, demonstrating the benefits of region guidance.  $L_{sms}$  achieves the best results, highlighting the advantage of selectively enforcing smoothness within specific regions. Notably, the full mask-aware approach (Method 3) shows improvement over basic mask guidance (Method 2), while  $L_{sms}$  delivers additional gains, validating the effectiveness of our selective gradient propagation strategy and underscoring the superiority of our ap-

Method	Smoothness Basis	RMSE	REL
1	I	0.163	0.027
2	M	0.159	0.028
3	M	0.148	0.024
4	M	0.141	0.023

Table 5. Comparison of different smoothness loss functions. **Smoothness Basis** indicates refers to the input used for gradient smoothness source: segmentation mask (M) or image (I). Methods 1.  $L_{smooth}$ : Uses the image as a guidance signal for smoothness. Method 2. Mask-Based  $L_{smooth}$ : Similar to  $L_{smooth}$  but utilizes a segmentation mask instead of the image. Method 3. **Mask-Aware Smoothness Loss**: Unlike  $L_{sms}$ , which uses only a subset of depth gradients within each region, this method incorporates all depth gradients for loss computation. Method 4.  $L_{sms}$ : Our proposed method.

Method	Auxiliary Input	RMSE	REL
1	I	0.158	0.027
2	M	0.141	0.023

Table 6. Comparison of different auxiliary inputs for self-supervised depth completion, Segmentation mask (M) or image (I)

proach in gradient optimization.

**Mask or Image?** To support self-supervised depth completion training, we introduce a segmentation branch as an auxiliary component. While ablation studies of  $L_{smooth}$  and  $L_{gc}$  suggest raw images can serve as auxiliary signals, we explore a purely image-based alternative by replacing segmentation masks with raw images in  $L_{smooth}$  and  $L_{gc}$ , alongside an image reconstruction loss. As shown in Table 6, the image-based method underperforms compared to the mask-based approach. Figure 4 demonstrates the image-based method fails to achieve comparable results with the mask-based method, whether on distinct (Figure 4a) or ambiguous textures (Figure 4b). This is due to excessive image textures misleading boundary identification, whereas segmentation masks provide clearer structural guidance for accurate depth completion. These findings have motivated us to adopt segmentation masks as the primary auxiliary component rather than relying on raw image data.

## 5. Conclusion

In this paper, we introduce selfDC, a novel self-supervised depth completion paradigm for image-guided depth completion. Our method relies solely on images and sparse depth measurements during training, with additional guidance from image segmentation masks, eliminating the need for dense depth labels. We analyze the depth completion process, where sparse depth measurements are propagated from observed points to neighboring

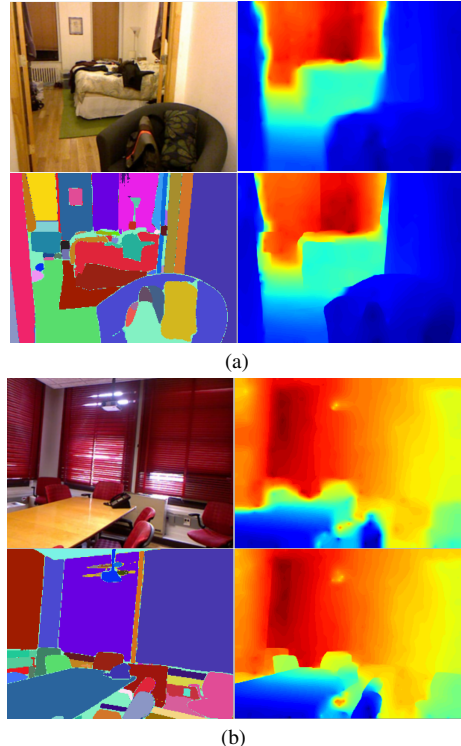


Figure 4. **Examples of depth predictions using different auxiliary inputs.** In (a) and (b), the top row shows depth prediction with image as auxiliary input, while the bottom row shows depth prediction with mask as auxiliary input.

regions, with depth maps exhibiting smoothness across the same object’s surface. Based on these observations, we propose the Local Gradient Constraint Loss and Selective Mask-Aware Smoothness Loss, enabling self-supervised depth completion without dense supervision. Our method achieves performance comparable to early supervised depth completion approaches and reaches SOTA results among self-supervised methods using geometric constraints from image sequences. While not yet matching the SOTA supervised methods, we believe this paradigm, reducing reliance on dense supervision, offers a more data-efficient and scalable solution. In semantic segmentation, semi-supervised methods with minimal supervision signals have long been a key research focus. We believe self-supervised depth completion, following a similar path, holds great potential for future advancements.

## References

- [1] Florent Bartoccioni, Éloi Zablocki, Patrick Pérez, Matthieu Cord, and Karteek Alahari. Lidartouch: Monocular metric depth estimation with a few-beam lidar. *Computer Vision and Image Understanding*, 227:103601, 2023. 1, 2, 4
- [2] Holger Caesar, Varun Bankiti, Alex H Lang, Sourabh Vora, Venice Erin Liong, Qiang Xu, Anush Krishnan, Yu Pan, Giancarlo Baldan, and Oscar Beijbom. nuscenes: A multi-

- modal dataset for autonomous driving. In *Proceedings of the IEEE/CVF conference on computer vision and pattern recognition*, pages 11621–11631, 2020. 1
- [3] Hu Chen, Hongyu Yang, Yi Zhang, et al. Depth completion using geometry-aware embedding. In *2022 International Conference on Robotics and Automation (ICRA)*, pages 8680–8686. IEEE, 2022. 2
- [4] Yun Chen, Bin Yang, Ming Liang, and Raquel Urtasun. Learning joint 2d-3d representations for depth completion. In *Proceedings of the IEEE/CVF International Conference on Computer Vision*, pages 10023–10032, 2019. 2
- [5] Xinjing Cheng, Peng Wang, and Ruigang Yang. Depth estimation via affinity learned with convolutional spatial propagation network. In *Proceedings of the European Conference on Computer Vision (ECCV)*, pages 103–119, 2018. 1, 2, 6
- [6] Xinjing Cheng, Peng Wang, and Ruigang Yang. Learning depth with convolutional spatial propagation network. *IEEE transactions on pattern analysis and machine intelligence*, 42(10):2361–2379, 2019.
- [7] Xinjing Cheng, Peng Wang, Chenye Guan, and Ruigang Yang. Cspn++: Learning context and resource aware convolutional spatial propagation networks for depth completion. In *AAAI 2020 - 34th AAAI Conference on Artificial Intelligence*, pages 10615–10622, 2020. 2, 6
- [8] Jaehoon Choi, Dongki Jung, Yonghan Lee, Deokhwa Kim, Dinesh Manocha, and Donghwan Lee. Selfdeco: Self-supervised monocular depth completion in challenging indoor environments. In *2021 IEEE International Conference on Robotics and Automation (ICRA)*, pages 467–474. IEEE, 2021. 1, 2, 4, 6
- [9] Rizhao Fan, Zhigen Li, Matteo Poggi, and Stefano Mattoccia. A cascade dense connection fusion network for depth completion. In *33rd British Machine Vision Conference 2022, BMVC 2022, London, UK, November 21-24, 2022*. BMVA Press, 2022. 1, 3
- [10] Rizhao Fan, Matteo Poggi, and Stefano Mattoccia. Contrastive learning for depth prediction. In *Proceedings of the IEEE/CVF Conference on Computer Vision and Pattern Recognition*, pages 3225–3236, 2023. 3
- [11] Rizhao Fan, Fabio Tosi, Matteo Poggi, Stefano Mattoccia, et al. Lightweight self-supervised depth estimation with few-beams lidar data. In *The 34th British Machine Vision Conference Proceedings*, pages 1–15. British Machine Vision Association’s (BMVA), 2023. 1, 2, 4, 5
- [12] Rizhao Fan, Matteo Poggi, and Stefano Mattoccia. Exploring few-beam lidar assistance in self-supervised multi-frame depth estimation. In *2024 IEEE/RSJ International Conference on Intelligent Robots and Systems (IROS)*, pages 2770–2777. IEEE, 2024. 2, 3
- [13] Ziyue Feng, Longlong Jing, Peng Yin, Yingli Tian, and Bing Li. Advancing self-supervised monocular depth learning with sparse lidar. In *Conference on Robot Learning*, pages 685–694. PMLR, 2022. 1, 2, 4
- [14] Andreas Geiger, Philip Lenz, and Raquel Urtasun. Are we ready for autonomous driving? the kitti vision benchmark suite. In *2012 IEEE conference on computer vision and pattern recognition*, 2012. 1, 5
- [15] Kaiming He, Xiangyu Zhang, Shaoqing Ren, and Jian Sun. Deep residual learning for image recognition. In *Proceedings of the IEEE conference on computer vision and pattern recognition*, pages 770–778, 2016. 5
- [16] Mu Hu, Shuling Wang, Bin Li, Shiyu Ning, Li Fan, and Xiaojin Gong. Penet: Towards precise and efficient image guided depth completion. In *2021 IEEE International Conference on Robotics and Automation (ICRA)*, pages 13656–13662. IEEE, 2021. 1, 2
- [17] Saif Imran, Yunfei Long, Xiaoming Liu, and Daniel Morris. Depth coefficients for depth completion. In *2019 IEEE/CVF Conference on Computer Vision and Pattern Recognition (CVPR)*, pages 12438–12447. IEEE, 2019. 6
- [18] Jitesh Jain, Jiachen Li, Mang Tik Chiu, Ali Hassani, Nikita Orlov, and Humphrey Shi. Oneformer: One transformer to rule universal image segmentation. In *Proceedings of the IEEE/CVF conference on computer vision and pattern recognition*, pages 2989–2998, 2023. 1, 3, 5
- [19] Xiaowen Jiang, Valerio Cambareri, Gianluca Agresti, Cynthia Ifeyinwa Ugwu, Adriano Simonetto, Fabien Cardinaux, and Pietro Zanuttigh. A low memory footprint quantized neural network for depth completion of very sparse time-of-flight depth maps. In *Proceedings of the IEEE/CVF Conference on Computer Vision and Pattern Recognition*, pages 2687–2696, 2022. 1
- [20] Diederik P Kingma. Adam: A method for stochastic optimization. *arXiv preprint arXiv:1412.6980*, 2014. 5
- [21] Alexander Kirillov, Eric Mintun, Nikhila Ravi, Hanzi Mao, Chloe Rolland, Laura Gustafson, Tete Xiao, Spencer Whitehead, Alexander C Berg, Wan-Yen Lo, et al. Segment anything. In *Proceedings of the IEEE/CVF International Conference on Computer Vision*, pages 4015–4026, 2023. 1, 3, 5
- [22] Jason Ku, Ali Harakeh, and Steven L Waslander. In defense of classical image processing: Fast depth completion on the cpu. In *2018 15th Conference on Computer and Robot Vision (CRV)*, pages 16–22. IEEE, 2018. 1
- [23] Ang Li, Zejian Yuan, Yonggen Ling, Wanchao Chi, Chong Zhang, et al. A multi-scale guided cascade hourglass network for depth completion. In *Proceedings of the IEEE/CVF Winter Conference on Applications of Computer Vision*, pages 32–40, 2020. 1, 2
- [24] Yuankai Lin, Tao Cheng, Qi Zhong, Wending Zhou, and Hua Yang. Dynamic spatial propagation network for depth completion. In *Proceedings of the aaai conference on artificial intelligence*, pages 1638–1646, 2022. 2, 5
- [25] Lina Liu, Xibin Song, Xiaoyang Lyu, Junwei Diao, Mengmeng Wang, Yong Liu, and Liangjun Zhang. Fcfr-net: Feature fusion based coarse-to-fine residual learning for depth completion. In *Proceedings of the AAAI Conference on Artificial Intelligence*, pages 2136–2144, 2021. 2
- [26] Sifei Liu, Shalini De Mello, Jinwei Gu, Guangyu Zhong, Ming-Hsuan Yang, and Jan Kautz. Learning affinity via spatial propagation networks. *Advances in Neural Information Processing Systems*, 30, 2017. 2
- [27] Xin Liu, Xiaofei Shao, Bo Wang, Yali Li, and Shengjin Wang. Graphcspn: Geometry-aware depth completion via

- dynamic gcns. In *European Conference on Computer Vision*, pages 90–107, Cham, 2022. Springer Nature Switzerland. 2
- [28] Ze Liu, Yutong Lin, Yue Cao, Han Hu, Yixuan Wei, Zheng Zhang, Stephen Lin, and Baining Guo. Swin transformer: Hierarchical vision transformer using shifted windows. In *Proceedings of the IEEE/CVF International Conference on Computer Vision*, pages 10012–10022, 2021. 2, 3
- [29] Fangchang Ma and Sertac Karaman. Sparse-to-dense: Depth prediction from sparse depth samples and a single image. In *2018 IEEE international conference on robotics and automation (ICRA)*, pages 4796–4803. IEEE, 2018. 2, 3, 5, 6
- [30] Fangchang Ma, Guilherme Venturini Cavalheiro, and Sertac Karaman. Self-supervised sparse-to-dense: Self-supervised depth completion from lidar and monocular camera. In *2019 International Conference on Robotics and Automation (ICRA)*, pages 3288–3295. IEEE, 2019. 1, 2, 4, 6, 7
- [31] Danish Nazir, Marcus Liwicki, Didier Stricker, and Muhammad Zeshan Afzal. Semattnet: Towards attention-based semantic aware guided depth completion. *arXiv preprint arXiv:2204.13635*, 2022. 1, 2
- [32] Jaesik Park, Hyeongwoo Kim, Yu-Wing Tai, Michael S Brown, and In So Kweon. High-quality depth map upsampling and completion for rgb-d cameras. *IEEE Transactions on Image Processing*, 23(12):5559–5572, 2014. 1
- [33] Jinsun Park, Kyungdon Joo, Zhe Hu, Chi-Kuei Liu, and In So Kweon. Non-local spatial propagation network for depth completion. In *European Conference on Computer Vision*, pages 120–136. Springer, 2020. 1, 2, 3, 5, 6
- [34] Adam Paszke, Sam Gross, Francisco Massa, Adam Lerer, James Bradbury, Gregory Chanan, Trevor Killeen, Zeming Lin, Natalia Gimelshein, Luca Antiga, et al. Pytorch: An imperative style, high-performance deep learning library. *Advances in neural information processing systems*, 32, 2019. 5
- [35] Jiaxiong Qiu, Zhaopeng Cui, Yinda Zhang, Xingdi Zhang, Shuaicheng Liu, Bing Zeng, and Marc Pollefeys. Deeplidar: Deep surface normal guided depth prediction for outdoor scene from sparse lidar data and single color image. In *Proceedings of the IEEE/CVF Conference on Computer Vision and Pattern Recognition*, pages 3313–3322, 2019. 2, 6
- [36] Nathan Silberman, Derek Hoiem, Pushmeet Kohli, and Rob Fergus. Indoor segmentation and support inference from rgb-d images. In *European conference on computer vision*, pages 746–760. Springer, 2012. 1, 5
- [37] Jie Tang, Fei-Peng Tian, Wei Feng, Jian Li, and Ping Tan. Learning guided convolutional network for depth completion. *IEEE Transactions on Image Processing*, 30:1116–1129, 2020. 2
- [38] Dennis Teutschner, Patrick Mangat, and Oliver Wasenmüller. Pdc: piecewise depth completion utilizing superpixels. In *2021 IEEE International Intelligent Transportation Systems Conference (ITSC)*, pages 2752–2758. IEEE, 2021. 1
- [39] Jonas Uhrig, Nick Schneider, Lukas Schneider, Uwe Franke, Thomas Brox, and Andreas Geiger. Sparsity invariant cnns. In *2017 international conference on 3D Vision (3DV)*, pages 11–20. IEEE, 2017. 1, 5, 7
- [40] Ashish Vaswani, Noam Shazeer, Niki Parmar, Jakob Uszkoreit, Llion Jones, Aidan N Gomez, Łukasz Kaiser, and Illia Polosukhin. Attention is all you need. *Advances in neural information processing systems*, 30, 2017. 2
- [41] Yufei Wang, Bo Li, Ge Zhang, Qi Liu, Tao Gao, and Yuchao Dai. Lrru: Long-short range recurrent updating networks for depth completion. In *Proceedings of the IEEE/CVF international conference on computer vision*, pages 9422–9432, 2023. 2
- [42] Yufei Wang, Ge Zhang, Shaoqian Wang, Bo Li, Qi Liu, Le Hui, and Yuchao Dai. Improving depth completion via depth feature upsampling. In *Proceedings of the IEEE/CVF Conference on Computer Vision and Pattern Recognition*, pages 21104–21113, 2024. 6
- [43] Alex Wong and Stefano Soatto. Unsupervised depth completion with calibrated backprojection layers. In *Proceedings of the IEEE/CVF International Conference on Computer Vision*, pages 12747–12756, 2021. 1, 6, 7
- [44] Alex Wong, Xiaohan Fei, Stephanie Tsuei, and Stefano Soatto. Unsupervised depth completion from visual inertial odometry. *IEEE Robotics and Automation Letters*, 5(2): 1899–1906, 2020. 1, 2, 7
- [45] Alex Wong, Safa Cicek, and Stefano Soatto. Learning topology from synthetic data for unsupervised depth completion. *IEEE Robotics and Automation Letters*, 6(2):1495–1502, 2021. 7
- [46] Yan Xu, Xinge Zhu, Jianping Shi, Guofeng Zhang, Hujun Bao, and Hongsheng Li. Depth completion from sparse lidar data with depth-normal constraints. In *Proceedings of the IEEE/CVF International Conference on Computer Vision*, pages 2811–2820, 2019. 2, 6
- [47] Zheyuan Xu, Hongche Yin, and Jian Yao. Deformable spatial propagation networks for depth completion. In *2020 IEEE international conference on image processing (ICIP)*, pages 913–917. IEEE, 2020. 2
- [48] Zhiqiang Yan, Kun Wang, Xiang Li, Zhenyu Zhang, Baobei Xu, Jun Li, and Jian Yang. Rignet: Repetitive image guided network for depth completion. *arXiv preprint arXiv:2107.13802*, 2021. 6
- [49] Zhiqiang Yan, Kun Wang, Xiang Li, Zhenyu Zhang, Jun Li, and Jian Yang. Desnet: Decomposed scale-consistent network for unsupervised depth completion. In *Proceedings of the AAAI conference on artificial intelligence*, pages 3109–3117, 2023. 1, 2, 6, 7
- [50] Zhiqiang Yan, Yuankai Lin, Kun Wang, Yupeng Zheng, Yufei Wang, Zhenyu Zhang, Jun Li, and Jian Yang. Tri-perspective view decomposition for geometry-aware depth completion. In *Proceedings of the IEEE/CVF Conference on Computer Vision and Pattern Recognition*, pages 4874–4884, 2024. 2
- [51] Yanchao Yang, Alex Wong, and Stefano Soatto. Dense depth posterior (ddp) from single image and sparse range. In *Proceedings of the IEEE/CVF Conference on Computer Vision and Pattern Recognition*, pages 3353–3362, 2019. 2, 6, 7
- [52] Sungho Yoon and Ayoung Kim. Balanced depth completion between dense depth inference and sparse range measurements via kiss-gp. In *2020 IEEE/RSJ International Con-*

- ference on Intelligent Robots and Systems (IROS)*, pages 10468–10475. IEEE, 2020. [1](#), [6](#), [7](#)
- [53] Yinda Zhang and Thomas Funkhouser. Deep depth completion of a single rgb-d image. In *Proceedings of the IEEE Conference on Computer Vision and Pattern Recognition*, pages 175–185, 2018. [1](#)
- [54] Youmin Zhang, Xianda Guo, Matteo Poggi, Zheng Zhu, Guan Huang, and Stefano Mattoccia. Completionformer: Depth completion with convolutions and vision transformers. In *Proceedings of the IEEE/CVF conference on computer vision and pattern recognition*, pages 18527–18536, 2023. [2](#)
- [55] Shanshan Zhao, Mingming Gong, Huan Fu, and Dacheng Tao. Adaptive context-aware multi-modal network for depth completion. *IEEE Transactions on Image Processing*, 30: 5264–5276, 2021. [1](#), [6](#)
- [56] Yiming Zuo and Jia Deng. Ogni-dc: Robust depth completion with optimization-guided neural iterations. In *European Conference on Computer Vision*, pages 78–95. Springer, 2024. [2](#)